

Adaptive Optics for Extremely Large Telescopes 4 – Conference Proceedings

Peer Reviewed

Title:
Aligning the LINC-NIRVANA Natural Guide Stars MCAO system

Journal Issue:
Adaptive Optics for Extremely Large Telescopes 4 – Conference Proceedings, 1(1)

Author:
Marafatto, Luca, INAF Padova
Baumeister, Harald, MPIA Heidelberg
Bertram, Thomas, MPIA Heidelberg
Berwein, Jurgen, MPIA Heidelberg
Briegel, Florian, MPIA Heidelberg
Bizenberger, Peter, MPIA Heidelberg
Herbst, Tom, MPIA Heidelberg
Hofferbert, Ralph, MPIA Heidelberg
Moreno-Ventas, Javier, MPIA Heidelberg
Kittmann, Frank, MPIA Heidelberg
Kuerster, Martin, MPIA Heidelberg
Bergomi, Maria, INAF Padova
Dima, Marco, INAF Padova
Farinato, Jacopo, INAF Padova
Ragazzoni, Roberto, INAF Padova
Viotto, Valentina, INAF Padova

Publication Date:
2015

Permalink:
http://escholarship.org/uc/item/2cr972kt

DOI:
http://dx.doi.org/10.20353/K3T4CP1131632

Local Identifier:
ao4elt4_31632

Abstract:
LINC-NIRVANA (LN) is an instrument built to be a Fizeau interferometric imager for the Large Binocular Telescope that will achieve ELT-like spatial resolution. Of course achieving this outstanding resolution requires a very complex instrument, assuring the delivery of plane wavefronts, parallel input beams, homoteticity and zero Optical Path Difference. LN will be one of the most complex ground-based instruments ever built, consisting of a Multi-Conjugate Adaptive

eScholarship
University of California

eScholarship provides open access, scholarly publishing services to the University of California and delivers a dynamic research platform to scholars worldwide.

Optics (MCAO) system, a fringe tracker, a beam combiner and a Near-InfraRed science camera, for a total of more than 250 indivudual lenses and mirrors.The MCAO sub-unit itself is the state of the art in the sector of wide field adaptive optics. It consists of 4 Wavefront Sensors (WFSs), two for each arm of the telescope, to sense the turbulence at the ground layer and at 7.1 km above the telescope. They operate in a layer oriented, Multiple Field of View mode, using up to 12 Natural Guide Stars (NGSs) for the ground layer correction and up to 8 NGSs for the mid layer correction.The ambitious nature of LN, which compels us to meet very tight requirements, together with the high number of subsystems lead to a challenging alignment procedure of the instrument. Despite of the complexity, the Alignment, Integration and Verification phase of the instrument has been recently completed with success in Heidelberg and LN is currently on its way to the LBT, where it will be re-aligned and finally mounted at one of the bend focal stations of the telescope. In this paper the integration and alignment procedure of the MCAO subsystem to the rest of LN is described and results are presented.

Copyright Information:

All rights reserved unless otherwise indicated. Contact the author or original publisher for any necessary permissions. eScholarship is not the copyright owner for deposited works. Learn more at http://www.escholarship.org/help_copyright.html#reuse



eScholarship
University of California

eScholarship provides open access, scholarly publishing services to the University of California and delivers a dynamic research platform to scholars worldwide.

Aligning the LINC-NIRVANA Natural Guide Stars MCAO system

Luca Marafatto[a,b], Kalyan Kumar Radhakrishnan Santhakumari[c], Thomas Bertram[c], Harald Baumeister[c], Maria Bergomi[a], Jurgen Berwein[c], Peter Bizenberger[c], Florian Briegel[c], Jacopo Farinato[a], Frank Kittman[c], Javier Moreno-Ventas[c], Tom Herbst[c], Roberto Ragazzoni[a], Valentina Viotto[a]

[a] INAF- Osservatorio Astronomico di Padova, [b] Università degli Studi di Padova, [c] Max Planck Institute fur Astronomie, Heidelberg

ABSTRACT

LINC-NIRVANA (LN) is an instrument built to be a Fizeau interferometric imager for the Large Binocular Telescope that will achieve ELT-like spatial resolution. Of course achieving this outstanding resolution requires a very complex instrument, assuring the delivery of plane wavefronts, parallel input beams, homoteticity and zero Optical Path Difference. LN will be one of the most complex ground-based instruments ever built, consisting of a Multi-Conjugate Adaptive Optics (MCAO) system, a fringe tracker, a beam combiner and a Near-InfraRed science camera, for a total of more than 250 indivudual lenses and mirrors.

The MCAO sub-unit itself is the state of the art in the sector of wide field adaptive optics. It consists of 4 Wavefront Sensors (WFSs), two for each arm of the telescope, to sense the turbulence at the ground layer and at 7.1 km above the telescope. They operate in a layer oriented, Multiple Field of View mode, using up to 12 Natural Guide Stars (NGSs) for the ground layer correction and up to 8 NGSs for the mid layer correction.

The ambitious nature of LN, which compels us to meet very tight requirements, together with the high number of subsystems lead to a challenging alignment procedure of the instrument. Despite of the complexity, the Alignment, Integration and Verification phase of the instrument has been recently completed with success in Heidelberg and LN is currently on its way to the LBT, where it will be re-aligned and finally mounted at one of the bend focal stations of the telescope. In this paper the integration and alignment procedure of the MCAO subsystem to the rest of LN is described and results are presented.

1 Introduction

LINC-NIRVANA (LN) is a very ambitious instrument that in its final configuration will allow to perform true interferometric imaging in a 10 x 10 *arcsec* FoV, with an equivalent spatial resolution of a 23 *m* telescope. [1]

To achieve this result LN is equipped with a complex multi-conjugate adaptive optics system, using solely Natural Guide Stars (NGSs), detecting and correcting the aberrations introduced in the wavefront by the ground layer and a high altitude layer (7.1 km) that would otherwise prevent the correct interferometric recombination of the light on the common focal plane.

More in detail, to perform MCAO correction, LINC-NIRVANA uses a pair of WFSs for each aperture of the telescope: the Ground layer Wavefront Sensor (GWS), detecting the turbulence introduced by the ground layer, and the High layer Wavefront Sensor (HWS), detecting the turbulence introduced at a height of 7.1 *km*.

The light coming from one arm of the telescope is split in two parts by an annular mirror: the annular portion of the beam, corresponding to a 2 – 6 *arcmin* FoV is reflected toward the entrance of the GWS, which uses up to 12 natural guide stars for wavefront sensing. The GWS is equipped with a bearing to compensate for the FoV rotation. The informations on the wavefront distortions retrieved by the GWS are sent to the adaptive secondary mirror of the LBT, equipped with 672 actuators, and the correction is performed at a maximum frequency of 1 KHz.

The central 2 *arcmin* are collimated, to avoid a separation of the PSFs in the common focal plane of the two arms of LBT. After the collimator, the beam is split by a dichroic into visible and IR light. The IR light is co-phased with the light coming from the other arm of the telescope by the so called piston mirror, a flat monolithic mirror, acting as the actuator for the fringe tracking loop. Such a recombination mirror compensates for the difference in path between the beams, producing in the interferomteric focal plane a fringe pattern. The scientific image forms on a CCD "HAWAII-2", 2048 x 2048 pixels, 0.005 *arcsec*/*pixel* located in a cryostat below the optical bench to minimize the thermal background.

The visible beam, 0.6 – 0.9 μm, inside the 2' FoV is re-focused by a F/20 optics at the entrance of the HWS, which uses up to 8 NGSs. The corrector for the high layer perturbations is a piezostack deformable mirror, conjugated at the same

height as the HWS, equipped with 379 actuators. To derotate the FoV of the HWSs two optical derotators, called K-mirrors, are inserted in the optical path toward the HWSs. The optics of LINC-NIRVANA consists of three functional groups: the warm collimator group (COL), the cold infrared optics (NIRCS) and the warm F/20 camera (FP20), used to deliver the light for wavefront sensing.

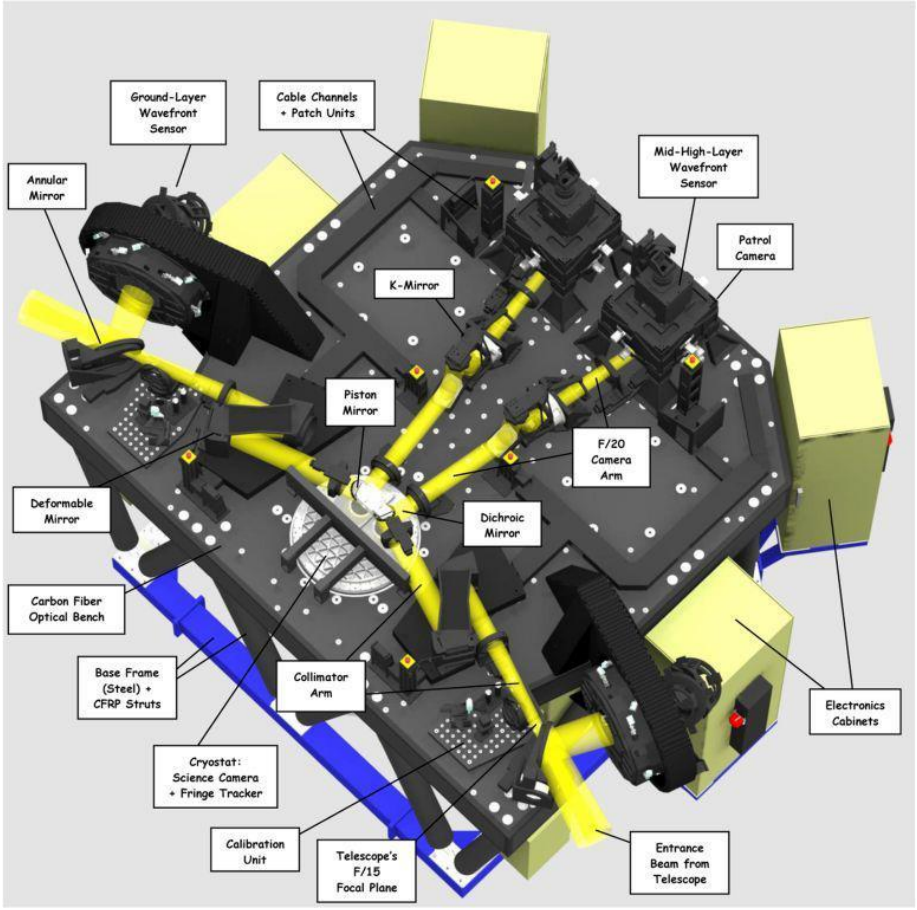


Figure 1: the optical bench of LINC-NIRVANA

In total the instrument contains 8 detectors, over 250 between lenses and mirrors, 2 deformable mirrors internal to the LN bench plus the two adaptive secondary mirror of the LBT driven by the GWSs, 133 motors and 40 control loops. Due to the high complexity of the instrument, which looks very much as an ELT instrument, the alignment strategy follows the philosophy to internally align the instrument in the lab first, and then align the telescope, through its secondary and tertiary mirror, to match the instrument. In this way it is possible to identify and solve problems before transporting the instrument to the mountain, where every task presents additional challenges and requires more time and extra effort. For this reason the instrument was almost completely aligned and tested before shipment to the LBT (one of the GWSs was not installed on the LN bench since it was at the LBT in the framework of a pathfinder experiment, described in [4] and [5]).
We describe here the alignment strategy and result of one of the two MCAO arms of LN, while for the alignment of the optics in the cryostat we refer to [6].

1.1 Alignment Sequence

The sequence of the individual alignment steps follows a logical order, scheduling manpower, lab space, critical equipment etc. to minimize idle time and the overall project development period. While some of the alignment procedures can run in parallel, others present dependencies from previous steps.
The conceptual sequence of the alignment is the following:

- Alignment of the piston mirror
- Alignment of the collimator axis
- Alignment of the powered collimator optics

- Alignment of FP20 axis
- Alignment of the K mirror
- Alignment of FP20 optics
- Alignment of the HWS
- Alignment of the GWS

For the description of the first 6 steps of the alignment we refer to [2], and we present here only the final result of the warm optics alignment, consisting of 6 lenses, 4 mirrors (1 deformable) and 1 filter. A FISBA interferometer simulates the telescope on-axis beam and is used as a reference for the alignment of the optics on the bench. When all the lenses are aligned, a spherical mirror is installed on the HWS structure, in order to have its center of curvature coincident with the focus of the FP20 optics, the light is reflected back into the interferometer and the wavefront is analyzed. In Figure 2 is shown the interferogram of the returned wavefront. The aberrations on the wavefront are less than 50 *nm* RMS, whose main contribution comes from the deformable mirror that, since it is deformable, can be shaped in a way to further minimize this value. However this value is already good thinking at the number of mirrors and lenses the light is passing through.
The residual tilt (6 fringes over a 126 *mm* diameter pupil translates into 3 *arcsec* tilt) is basically impossible to remove due to the limited adjustment accuracy for tip-tilt of the lenses mounts.

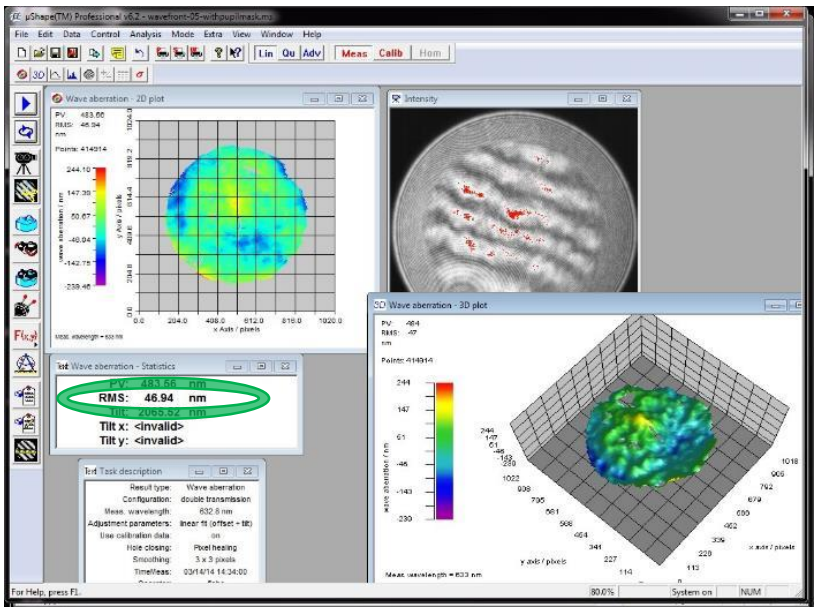


Figure 2: Interferogram of the returned wavefront after passing the warm optics

2 HWS Alignment

The HWS is a multi-pyramids WFS that uses up to 8 reference stars, acquired by 8 Star-Enlargers (SE) [3], and works in layer oriented mode.
Each HWS drives a deformable mirror equipped with 349 actuators, internal to the LINC-NIRVANA bench, conjugated to the same height.
The incoming beam delivered by the warm optics is a F/20, flat and telecentric, and is derotated by the K-mirror. The light from the reference stars passes through the SEs and a pupil re-imager (constituted of a 7 lenses objective with 112 *mm* aperture and 99 *mm* focal length, resulting in a very fast F/0.88 optics) re-creates the images of the telescope entrance pupil on a 80 x 80 pixels, 24μm pixelsize, E2V CCD39.
The HWS alignment basically consists in centering its CCD to the on axis reference beam, conjugate it to the proper height and co-align the 8 SEs in tip-tilt and focus to avoid incorrect overlap of the pupils on the detector.
Since the HWS works with up to 8 stars distributed on a 2 *arcmin* FoV while the FISBA beam simulates only an on-axis star, the alignment of the HWS cannot be fully accomplished just using the FISBA beam, but it relies on the previous alignment of a fiber plate (which is part of the calibration unit of the instrument) containing 23 fibers, 1 on-axis and 22 off-axis evenly distributed over a 2 *arcmin* FoV.
In turn, the alignment of the fiber plate cannot be performed before a preliminary partial alignment of the HWS to the on-axis reference beam, leading to a multi-steps alignment procedure.

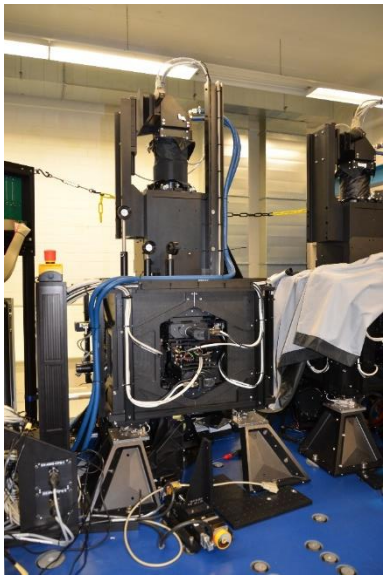


Figure 3: the High layer Wavefront Sensor

2.1 Alignment of the lateral position of the CCD39

A mask with a small central hole is inserted in the light path, at the pupil plane. No SEs are inserted in the path, so the light enters the HWS passing directly through its pupil re-imager and is imaged on the CCD. The CCD is moved on its plane till the centroid of the spot produced by the on-axis beam falls at the center of the CCD. However, because of the non-perfect perpendicular mounting of the CCD stages, a motion along the optical axis shifts the spot also in X and Y direction. The lateral position is then re-adjusted after the CCD is focused to the pupil plane.

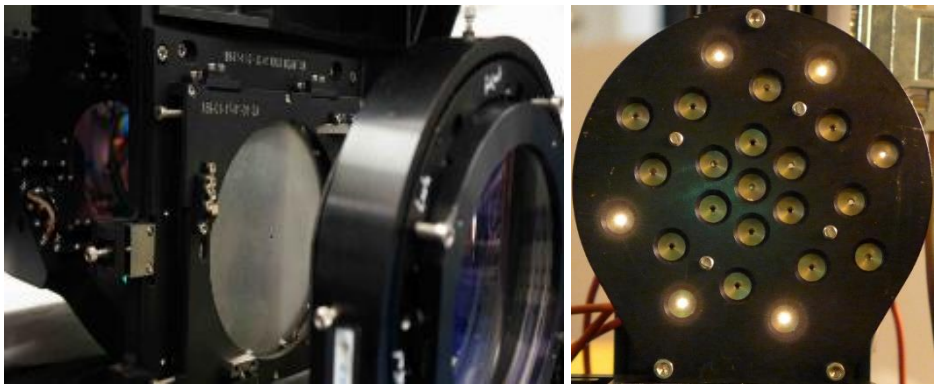


Figure 4: on the left the mask with a 2 mm central hole positioned in the pupil plane, used for the CCD39 centering and conjugation to the pupil plane and for the SEs tip-tilt alignment. On the right the fiber plate containing 23 fibers (1 on-axis) distributed in a 2 arcmin FoV, used during the HWS alignment.

2.2 CCD conjugation to the pupil plane

The CCD is initially conjugated to the pupil plane rather than to its correct conjugation height, to ease and speed up the alignment of the SEs of the HWS. In fact, when the CCD is conjugated to the pupil the images of the pupil produced by each SE are perfectly superimposed on the detector, if all the SEs are perfectly co-aligned. Misalignment between SEs leads to a relative displacement of the pupil images on the CCD, which can be easily evaluated when the CCD is conjugated to the pupil, since all the pupils should have the same barycenter position. On the other hand, when the CCD is conjugated to a different height, the pupil images superposition on the detector is only partial, resembling the superposition of the reference stars footprints occurring in the atmosphere at the conjugation height. Therefore, even when the SEs are perfectly aligned, the barycenters of the pupil images produced by each SE on the detector fall on different pixels. The CCD conjugation to the pupil plane is done using more than one fiber (we used 4) of the fiber plate, whose

light passes through the PR-I of the HWS and is focused on the CCD. The CCD is optically conjugated to the pupil plane when the spots produced by each fiber perfectly overlap with the ones produced by the other fibers. The fact that the fiber plate is not yet aligned to the reference beam has a negligible effect in this phase, provided that the light from the fibers used at this stage passes through the PR-I. Once the CCD is properly focused to the pupil plane, its lateral position is adjusted as described before.

2.3 Preliminary alignment of the SEs tip tilt

The 8 SEs of the HWS are then pre-aligned in tip-tilt, a step necessary for the tip-tilt alignment of the fiber plate. At this point the only reference source is the on axis beam of the FISBA, so first of all we checked that all the SEs could reach the reference beam, which is at the edge of their travel ranges, and verified that the pyramid rotation angle of each SE was aligned with the CCD rows/columns to 0.1 pixel. Each SE is then finely centered on FISBA PSF. This operation is performed removing the mask in the pupil plane so that the SE is receiving the whole beam and produces on the CCD 4 images of the pupil. The SE is correctly centered on the reference beam when the 4 pupils are equally illuminated. For the SE tip-tilt alignment the holed mask is introduced in the path, in order to have 4 small spots on the CCD instead of 4 big pupil images, to facilitate the completion of this task (it is easier and more accurate computing a centroid on a small spot rather than on a big one). The goal of the alignment is to obtain, for each SE, that the centroid of the 4 spots produced by all the SE falls on the same CCD pixels, namely pixel (20, 20) of each CCD quadrant, with a maximum discrepancy of 0.1 pixels. When this result is achieved, all the SEs are well co-aligned in tip-tilt and can be used as a reference for the tip-tilt alignment of the fiber plate.

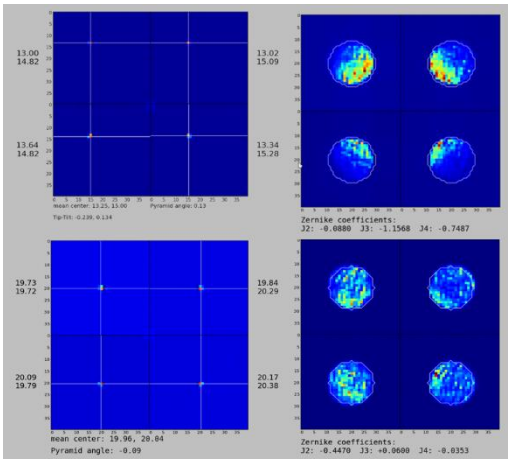


Figure 5: in the top panels the signatures on a mis-aligned SEs. On the left the four small spots produced by a SE used for the tip tilt alignment. On the right the four pupils produced by a SE used for its focus alignment (a clear intrs-focus signal is visible in the top-right panel). In the bottom panel the signatures of an aligned SE (centroids of the 4 spots on the right pixel within the requirements and pupils evenly illuminated).

2.4 Fiber plate Alignment

As stated before the fiber plate is constituted of 23 fibers, displaced on a 2 *arcmin* FoV, inserted in a curved aluminum plate to simulate the curved FoV (FP15), delivered from the LBT, entering the LN bench. Its alignment to the reference beam is crucial to refine the alignment of the HWS SEs. The initial step is to align the central fiber to the telescope focal plane as defined by the FISBA beam. A flat mirror in the calibration unit, with the possibility to rotate, is positioned so to reflect the light from the central fiber of the fiber plate into the main beam beam of the telescope, toward the HWS. A SE is positioned on axis, intercepting the light of the FISBA beam and producing 4 equally illuminated pupil images on the detector. The FISBA is then switched off and the fiber plate is moved, thanks to its motorized stages, initially on its XY plane until the PSF produced by the central fiber is perfectly centered on the on-axis SE, and then in Z axis to minimize the focus term measured by the WFS. The central fiber of the fiber plate is now aligned to the FISBA beam. Four different SEs are then centered, one at the time, on the on axis fiber and aligned in focus adjusting the focus mechanism of the SEs,

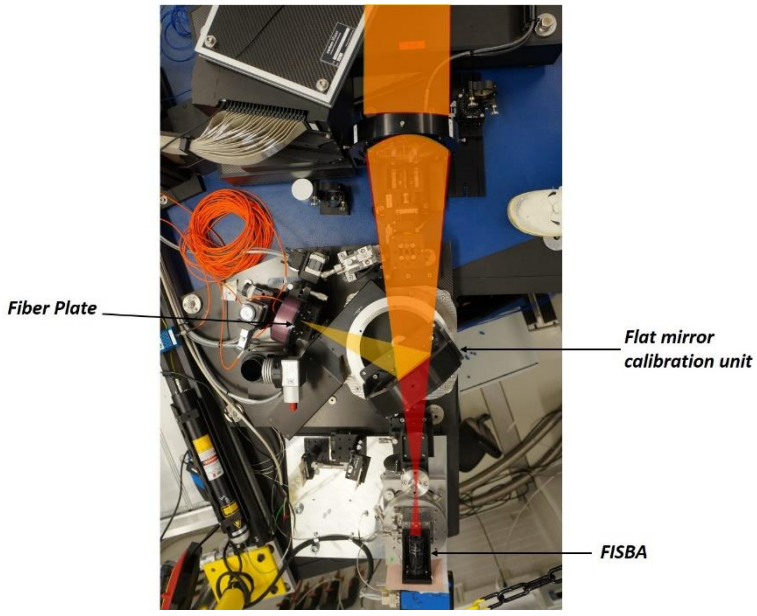


Figure 6: Reference light sources area. The fiber plate on-axis beam (yellow) is co-aligned to the reference FISBA beam (red) translating the fiber plate and rotating the flat mirror of the calibration unit.

minimizing the defocus term measured by the HWS. The same 4 SEs are used for the tip-tilt alignment of the fiber plate, achieved with an iterative procedure centering the aligned SEs on the on axis and off axis fibers.

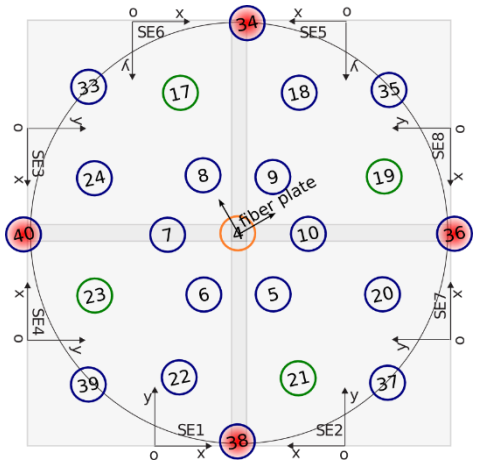


Figure 7: coarse positions of the fibers on the fiber plate. The circle represents the 2 arcmin FoV, the different squares represent the areas spaned by different SEs. The central fiber is reachable by all the SEs. The tip tilt alignment of the fiber plate was done on the green positions (fibers #17, #19, #21 and #23). The fibers in red were not reachable by any SE since the outermost fiber ring of the fiber plate has a diameter that proved to be slightly larger than the diameter corresponding to the 2 arcmin FoV.

Since the curved focal plane delivered from the LBT is flattened at the HWS entrance by the FP20 optics, the fiber plate tip tilt alignment is performed by simply minimizing the focus gradient along each tilt axis by tilting the fiber plate. When the defocus signals measured by the 4 SEs on various fibers in different FoV (#17, #19, #21 and #23 in Figure 7) positions are the same, the fiber plate is aligned and the absolute focus is adjusted by moving it along Z direction to minimize the defocus signal. What we measured at the beginning was a symmetric defocus gradient across the FoV, indicating that the fiber plate was correctly aligned in tip-tilt but the HWS entrance focal plane was not flat as it was supposed to be. This problem could derive from: a wrong curvature of the fiber plate, some effects introduced by the FP20 optics or an inclination of the linear stages moving the SEs. To investigate this problem we moved the fiber plate on a plane perpendicular to the optical axis of known amounts (8.25 *mm*). The fact that the fiber plate is curved, to mimic the curvature of the entrance FoV (FP15), and we are moving it on a plane translates into an axial shift of the sources, depending on their position in the fiber plate and on the lateral shift applied to it.

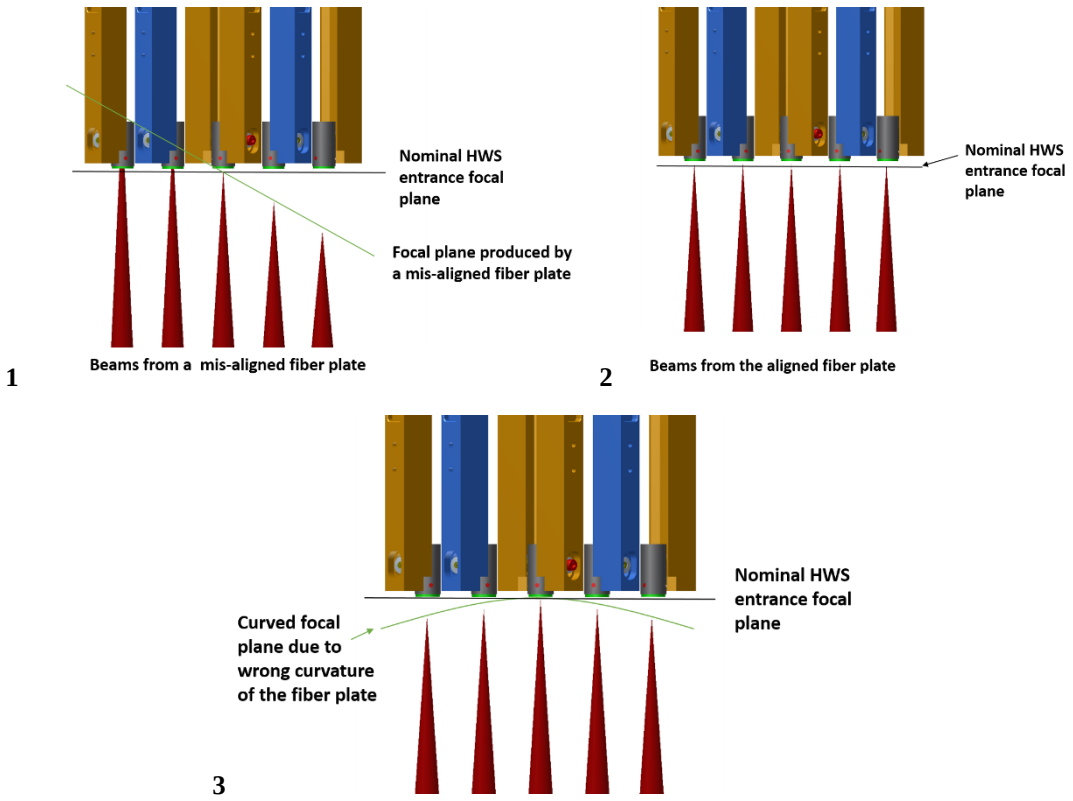


Figure 8: In panel 1 is depicted a focal plane delivered by a tilted fiber plate (the effect is here greatly magnified). In panel 2 the focal plane when the fiber plate is perfectly aligned. In panel 3 a representation of the initial result of the alignment (again the effect here is greatly magnified). The fiber plate is well aligned in tip tilt but the delivered focal plane shows a residual curvature, probably due to a wrong curvature of the fiber plate.

Knowing these parameters and the curvature radius of the FP15 we derived the expected defocus signals for different shifts of the fiber plate The measured values are then compared with the expected ones.
The expected focal shifts resulting from these lateral displacements of the fiber plate are:

- - 0.19 *mm* in FP15 coordinates (0.25 *mm* in FP20) for a shift of -8.25 *mm*, giving a defocus signal on the HWS, in arbitrary units, of - 0.17.
- + 0.25 *mm* in FP15 coordinates (0.33 *mm* in FP20) for a shift of +8.25 *mm*, giving a defocus signal on the HWS, in arbitrary units, of + 0.23.

Measured results:

- -0.1 arbitrary units
- +0.1 arbitrary units

Due to vibrations, the precision in measuring the defocus signal with our setup was ~ 0.05 arbitrary units. This test is basically insensitive to the fiber plate curvature, while it measures a possible defocus signals introduced by the FP20 lenses and inclinations of the SEs linear stages. Since the result of the test is almost consistent with our expectations, and anyhow below the relative focus alignment tolerance for the SEs of 0.15 arbitrary units, we concluded that FP20 lenses and SEs linear stages are working as expected, unless the very unlucky and unlikely case they are compensating each other.
The different focus signals measured moving a SE on and off-axis was then considered mainly as the result of a wrong curvature of the fiber plate, that was redesigned, reworked and tested. The new fiber plate reduced the residual curvature at the HWS entrance focal plane, and even if it is not completely eliminated this parameter is now within the requirements.

2.5 SEs fine alignment

Once the fiber plate is aligned we had a large number of fibers available to refine the SEs tip-tilt and focus alignment. Since the linear stages moving the SEs are affected by pitch, roll and yaw, to minimize their effects on the pupil images,

the idea is to move each SEs to the middle of its travel range and then to center it to the closest fiber for tip-tilt and focus alignment.
The tip-tilt alignment concept is the same described in the paragraph of the SE preliminary alignment. The SE focus alignment is performed shifting the whole SE along the optical axis to minimize the defocus signal measured by the HWS. The goal is to have, for all the SEs, a residual wavefront error due to the defocus term of less than 20 *nm*, corresponding to 0.15, arbitrary units, in our measurement system. The results of the alignment are presented in Table 1, showing the requirements have been succesfully met for all the SEs.

SE	***Defocus [nm WFE]***	***Tip-Tilt (mean center)***
SE01	7	20.09, 19.99
SE02	20	20.03, 19.98
SE03	4	20.03, 19.97
SE04	4	19.97, 20.02
SE05	10	20.00, 20.00
SE06	2	20.05, 20.03
SE07	20	20.01, 20.06
SE08	3	20.00, 20.01
GOAL	**20**	**(20.00, 20.00) ± 0.1**

Table 1: Results of the HWS SEs fine alignment.

2.6 CCD conjugation to the deformable mirror

To conclude the alignment of the HWS, the CCD39 was conjugated to the correct altitude. A holed mask is located as close as possible to the optical surface of the deformable mirror, which is optically conjugated to the required altitude of 7.1 *km*. One SE is centered on the on-axis fiber and another SE is centered on an off-axis fiber, the CCD is then moved along the optical axis until the spots produced by the 2 SEs overlap on the detector.

3 GWS alignment

The GWS is constituted of a references selection unit, in which up to 12 SEs are moved in the 2 – 6 *arcmin* annular FoV to select the guide stars and a PR-I, whcich is basically a folded Schmidt-camera. The beams coming from the SEs are firstly reflected by a flat annular folding mirror and then focused by a parabolic mirror toward a 4-lenses objective, re-imaging the 4 pupils on the CCD. The detector is a CCD50 128 × 128 pixels, 24 *μm* pixelsize, mounted on the rear of the Pupil Re-Imager, on a remotely controllable XYZ linear stage.

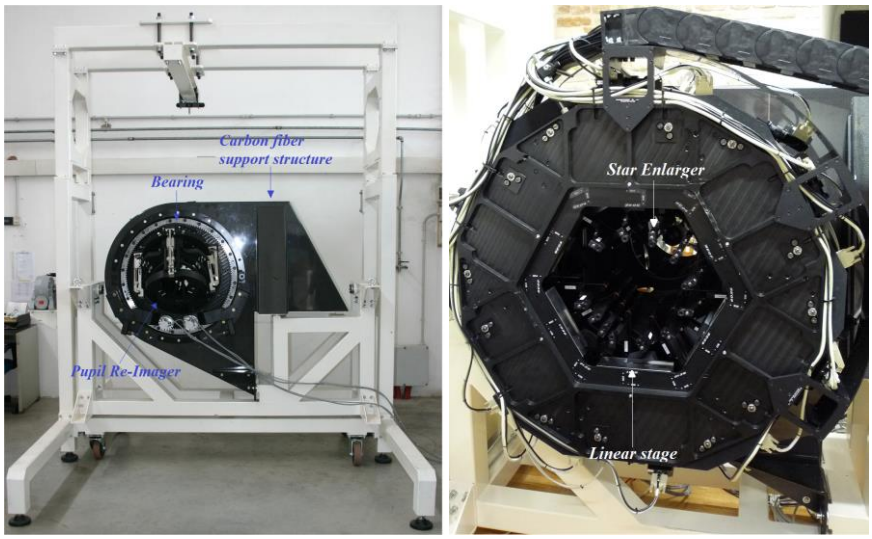


Figure 9: the Ground layer Wavefront Sensor

The whole unit is mounted on a rotation unit to follow the sky. Essentially, it is a bearing with the purpose to mechanically rotate the whole GWS in order to compensate for the field rotation.

An annular mirror folds the outer 2-6 *arcmin* FoV into the sensor. Since the Annular Mirror (AM) is the only LN optics before the entrance of the GWS, the internal alignment of this sensor has no dependencies from the previous alignment of other subsystems, differently from the HWS, so that it can be performed separately, in parallel with other activities. The internal alignment of the GWSs has been performed in Padova at INAF premises, the procedure and the results are widely discussed in [7] and [8].
Once the GWS is internally aligned we aligned it to the rest of the instrument's optics. For this purpose a F/15 light source (called "Magic Lantern") is placed in front of the annular mirror. To span the complete GWS FoV the Magic Lantern is equipped with three linear translation stages for movement in X, Y and Z axes. To place this source at the correct coordinates, the feedback signal (tilt and defocus) from the HWS is used. The AM mount features 1 tilt stage, 1 rotation stage and a translation stage (along the optical axis), the response from the GWS is used to adjust the AM. Any residual misalignment that cannot be compensated with the AM has to be adjusted by shimming the whole GWS.
In the follwing the GWS alignment concept and results are presented.

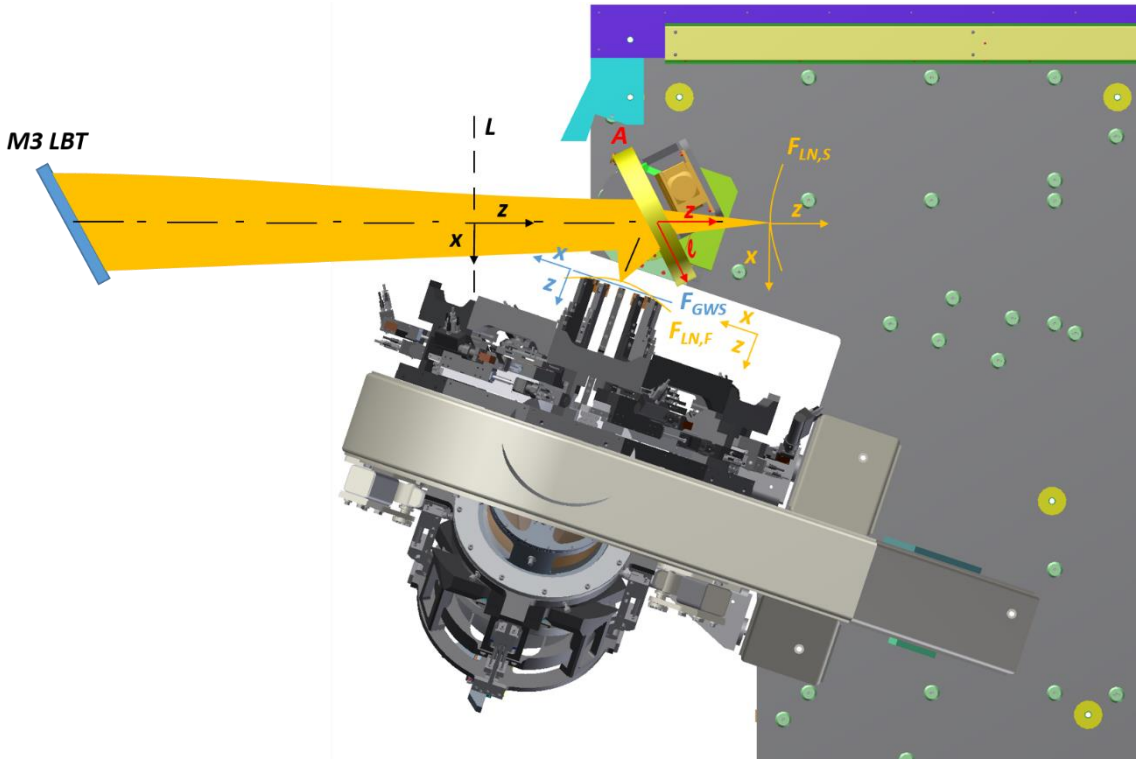


Figure 10: sketch of the relevant reference planes for the GWS alignment to the rest of LN.The y axis, not shown here, is always directed toward the reader.

- **$F_{LN,S}$:** the straight LN internal F/15 focal plane to which the full instrument arm is aligned to. The straight telescope focal plane has to coincide with **$F_{LN,S}$**
- **$F_{LN,F}$:** the folded LN internal F/15 focal plane is defined by **$F_{LN,S}$** and the position and orientation of the AM
- **F_{GWS}** : the GWS internal focal plane, defined by the common nominal focus of the SEs and the rotation axis of the GWS bearing.
- **A**: Annular Mirror surface with the origin in the pivot point of the AM, directions y and l in the surface of the mirror, z in direction of straight light propagation.
- **L**: plane parallel to the tangential plane passing through the vertex of **$F_{LN,S}$** but in front of the AM. The Magic Lantern is positioned along this plane.

The goals of the alignment are:

- Minimize the tilt of **$F_{LN,F}$** with respect to **F_{GWS}**
- Minimize the difference of the focus position of **$F_{LN,F}$** and **F_{GWS}** over the entire 2 – 6 *arcmin* FoV.
- Minimize the decentering effect, i.e. reduce separation of the centers of **$F_{LN,F}$** and **F_{GWS}** in x and y directions.

After having made the ML parallel to the nominal optical axis of the LN arm (z-axis of **L** reference frame co-aligned with z-axis of **$F_{LN,S}$** reference frame), looking at the positions of the pupils produced on the HWS, we tested the possibility to

align the AM tip-tilt using the position of the pupils on the CCD50 of the GWS as a reference. To do this we performed the following steps:

- The Magic Lantern is positioned at [0, 68] *mm* in the $\mathbf{F_{LN,F}}$ x-y coordinate system .
- SE07 is positioned at [0, 68] *mm* in the $\mathbf{F_{GWS}}$ x-y coordinate system.
- The AM tip-tilt has been adjusted in order to center the pupils on the CCD50 with 1 pixel precision, equal to 24 μm

A shift of the pupils on the CCD50 of 1 pixel corresponds to a tilt of the AM of :

$$Tilt = \frac{1}{2} \cdot \frac{k}{f_{PR-I}} \cdot Pupil\ shift\ on\ CCD \cdot 206265''$$

Where $f_{PR\text{-}I}$ is the equivalent focal lenght of the GWS Pupil Re-Imager and k is the star enlerger enlarging factor. Since, in our system, $f_{PR\text{-}I}$ = 223.9 *mm* and k = 12.5, the AM is aligned with respect to the GWS optical axis with a precision better than 138''. Using a centroid routine to measure the pupils positions with sub-pixel accuracy the precision could be easily improved of one order of magnitude.
The AM was homed several times and moved back to the same position to check its positioning repeatability, which resulted to be extremely good.
For the AM focus alignment the defocus signal measured by the GWS was used. As for the AM tip-tilt alignment SE07 was moved at position [0, 68] *mm* in the $\mathbf{F_{GWS}}$ x-y coordinate system and the Magic Lantern was centered on SE07, so to obtain 4 equally illuminated pupils. To reduce the defocus term measured through SE07 the AM was shifted along the LN optical axis, with SE07 tracking the beam at the same time. This happens because focus compensation with the AM introduces a lateral shift of $\mathbf{F_{LN,F}}$. The same was done using three other SEs positioned on a cross pattern on a circle 0f 68 *mm* in radius. Their positions are listed in Table 2.

	SEs starting position	**SEs focused position**	**Delta**
SE01	[0, -68] mm	[-6.1, -66.5] mm	[-6.1, 1.5] mm
SE03	[-68, 0] mm	[-75, 1.9] mm	[-7, 1.9] mm
SE07	[0, 68] mm	[-6.1, 70] mm	[-6.1, 2] mm
SE09	[68, 0] mm	[61, 1.5] mm	[-6, 1.5] mm

Table 2: positions of the SEs in the F_{GWS} x-y coordinates system before focusing the AM (SEs starting position) and after focusing the AM (SEs focused position). On average, to get focused pupils from the SEs we had to shift them by 6 mm in X axis and 2 mm in Y axis in the F_{GWS} coordinates system.

The result is that, to compensate the offset in focus between $\mathbf{F_{GWS}}$ and $\mathbf{F_{LN,F}}$ we introduced a lateral shift of $\mathbf{F_{LN,F}}$ wrt $\mathbf{F_{GWS}}$ of about 6 *mm* in the X axis and 2 *mm* in the Y axis..



Figure 11: position of the SEs used for tip-tilt and focusing alignment of the AM, as seen from in front of the GWS entrance. The SEs were initially positioned on a cross pattern (blue circles) on a circle 68mm in radius, centered on the nominal center of the GWS focal plane. The pupils we got in these positions were highly defocused, so we moved the AM in focus, tracking the beam at the same time with the SEs. The red circles represent the positions of the SEs where we had, at a visual inspection, pupils with no defocus signal. The final positions of the SEs are shifted, on average, of 6mm in X axis and 2mm in Y axis wrt the starting position

To double-check this result in a different way, the Magic Lantern was positioned at [0, 68] *mm* in the $\mathbf{F_{LN,F}}$ focal plane and SE07 was centered onto the ML spot, corresponding to position [-6.17, 69.866] *mm* in the $\mathbf{F_{GWS}}$ focal plane, with the

bearing at 0°. The bearing was then rotated of ±60° in steps of 15°, and at the same time the ML was displaced simulating a rotating FoV. For each position of the bearing, the discrepancy between the ML spot position in the $\mathbf{F_{LN,F}}$ focal plane and the SE position translated in the $\mathbf{F_{GWS}}$ focal plane has been recorded.
Considering the range [-30°, +30°] of bearing rotation, the mean offset between the centers of $\mathbf{F_{GWS}}$ and $\mathbf{F_{LN,F}}$ we measured was [-6.2, 1.96] *mm*, confirming what measured during the AM focus alignment. The 2 *mm* offset in Y axis can be compensated by incresing the shims under the GWS, while the 6 *mm* offset in X direction cannot be really compensated since the only way to reduce it would be moving the AM along the optical axis, consequently introducing an offset in focus, or a very invasive remachining of the SEs.

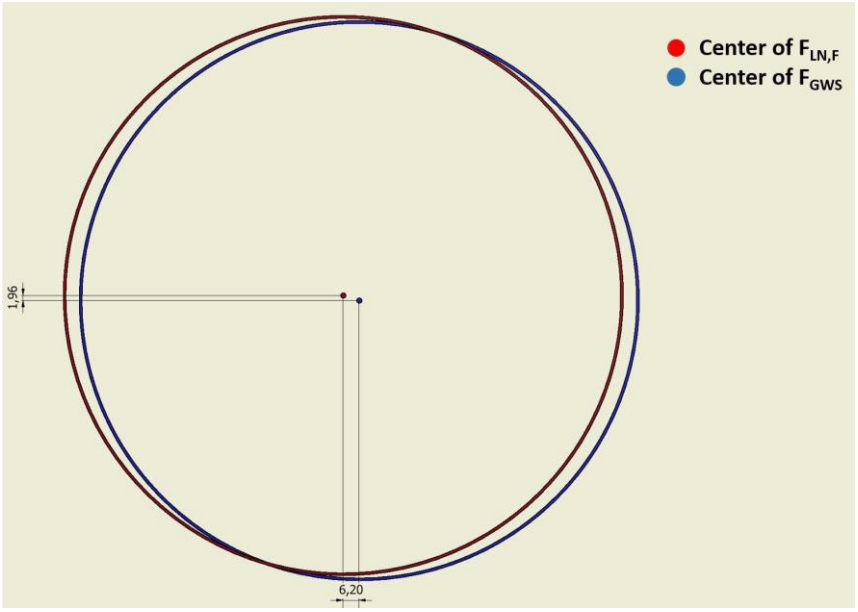


Figure 12: decenter between the $F_{LN,F}$ and the F_{GWS}

During investigations to understand the cause of this large offset between $\mathbf{F_{GWS}}$ and $\mathbf{F_{LN,F}}$ focal planes, it was found that the GWS is 5.4 *mm* closer to the center of the LN reference sphere (representing the on-axis focus position of $\mathbf{F_{LN,S}}$) than what expected from the drawings. The reason of this discrepancy was found to be due to an incorrect positioning of the reference sphere that was shifted 4.3 *mm* toward the $\mathbf{F_{GWS}}$ from its nominal position, which lead to a misplacement of the same amount of the FISBA beam simulating the telescope on-axis beam and used for the alignment of the warm optics and of the HWS.
This lateral misalignment affected only the optics before the pupil plane internal to LN bench, and therefore, other than the GWS, mainly the collimator optics. This problem was readily solved by re-aligning them with the correct reference beam, while the GWS was not re-aligned, since this alignment was basically to demonstrate the validity of the GWS to bench alignment procedure and it must be anyhow dismounted from the bench for the shipment to the LBT and re-aligned at the telescope.

4 Conclusions

Aligning an instrument with such a complexity, number of subsystem and degrees of freedom presents unique challanges. Numerous issues have been considered in advance in the alignment procedure and in the sequence of events, enabling a procedure that proved to be robust and lead to the succesful alignment of the MCAO module in the lab, allowing at the same time to detect some issues and problems, readily resolved in the lab but whose detection on the mountain would have taken a much longer time and effort.
Also in light of these results, the instrument successfully passed the Preliminary Acceptance Europe review and was finally shipped, divided in several boxes and containers, to the LBT, where the instrument will be re-integrated and re-aligned and finally commissioned. These operations, preliminary to the instrument installation on the telescope, despite the complexity of the instrument and the long time required for the alignment in the lab (just the alignment of the MCAO arms took almost one year), are expected to require roughly 130 days of work, divided in several runs, taking advantage

of the experience acquired in the lab and of the pins located on LN bench to accurately reposition various lenses and mirrors of the instrument, removed before the shipment for safety reasons.

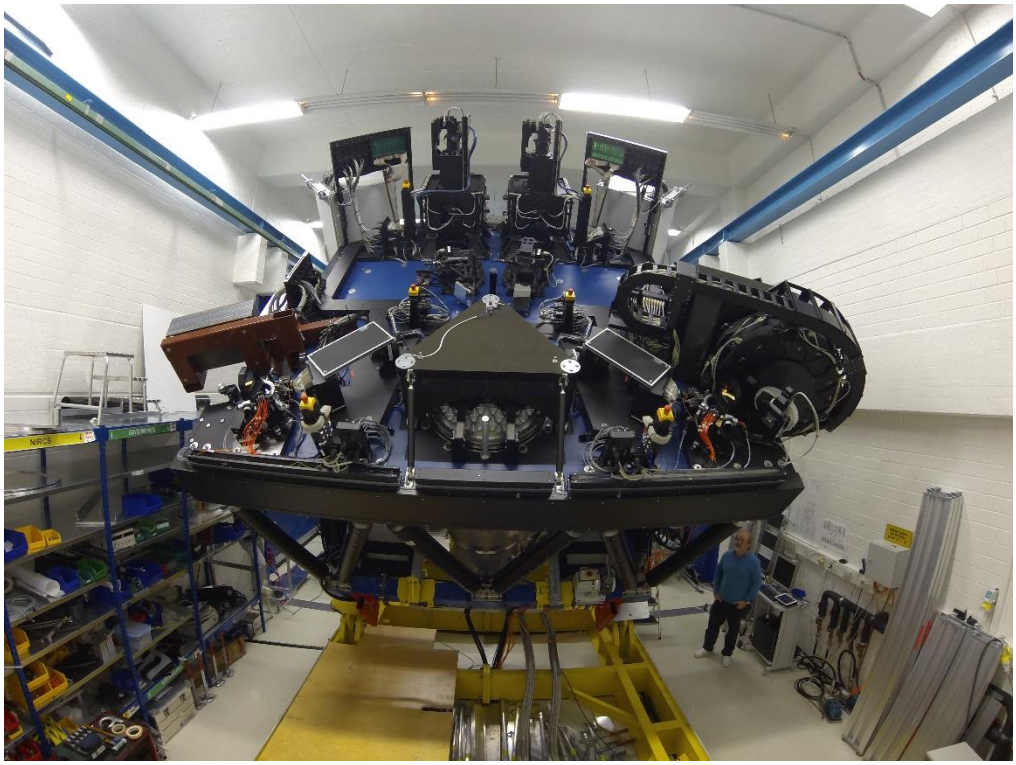


Figure 13: the whole instrument fully integrated and aligned during flexures test in Heidelberg. The GWS on the left side in this picture was replaced by a dummy mass, since the real sensor was mounted at LBT for a Pathfinder Experiment.

5 References

1. Herbst T.M., Ragazzoni R., Andersen D., Bhnhardt H., Bizenberger P., Eckart A., Gaessler W., Rix H.W., Rohloff R.R., Salinari P., Soci R., Straubmeier C., Xu W., "LINC-NIRVANA, a Fizeau beam combiner for the Large Binocular Telescope", Proc. SPIE 4838, 456-465 (2003).
2. Moreno-Ventas, J., Baumeister, H., Bertram, T., Bizenberger, P., Briegel, F., Greggio, D., Kittmann, F., Marafatto, L., Mohr, L., Radhakrishnan, K., and Schray, H., "Optical Integration and verification of LINC-NIRVANA," Proc. SPIE 9147, 9147146 (2014).
3. Ragazzoni R., Diolaiti E., Vernet E., Farinato J., Marchetti E. and Arcidiacono C., "Arbitrarily Small Pupils in Layer-Oriented Multi-Conjugate Adaptive Optics", *ASP* **187**, p. 860, 2005.
4. Bergomi, M., Viotto, V., Arcidiacono, C., Baumeister, H., Bertram, T., Berwein, J., Briegel, F., Conrad, A. R., Farinato, J., Herbst, T. M., Hofferbert, R., Kopon, D., Kittman, F., Marafatto, L., and Ragazzoni, R., "First light of the LINC-NIRVANA Pathfinder experiment," Proc. SPIE 9148, 9148106 (2014).
5. Kopon, D. A., Conrad, A. R., Bertram, T., Herbst, T., Berwein, J., Ragazzoni, R., Farinato, J., Viotto, V., Bergomi, M., Marafatto, L., Kittmann, F., Rohloff, R.-R., Baumeister, H., De Bonis, F., Hofferbert, R., Arcidiacono, C., Puglisi, A. T., Brunelli, A., Pott, J.-U., Bizenberger, P., Briegel, F., Kürster, M., Meschke, D., Mohr, L., and Zhang, X., "Pathfinder First light: alignment, calibration, and commissioning of the LINC-NIRVANA ground-layer adaptive optics subsystem," Proc. SPIE 9148, 914877 (2014).
6. Bizenberger P., Baumeister H., Fopp P., Herbst T., Laun W., Mohr L., Moreno-Ventas J., "LINC-NIRVANA: Diffraction limited optics in cryogenic environment", Proc. SPIE 9147, 9147B-1 (2014)
7. Marafatto L., Bergomi M., Brunelli A., Dima M., Farinato J., Farisato G., Lessio L., Magrin D., Ragazzoni R., Viotto V., Bertram T., Bizenberger P., Briegel F., Conrad A., DeBonis F., Herbst T., Hofferbert R., Kittmann F., Kuerster M., Meschke D., Mohr L., Rohloff R.R., "Aligning a more than 100 degrees of freedom wavefront sensor", Proc. SPIE 8447, 84476F-1 (2012).
8. Kumar Radhakrishnan Santhakumari, K., Marafatto, L., Bergomi, M., Viotto, V., Farinato, J., Ragazzoni, R., Herbst, T. M., Bertram, T., Dima, M., Bizenberger, P., Briegel, F., Kittmann, F., Mohr, L., and Magrin, D., "Ground layer correction: the heart of LINC-NIRVANA," Proc. SPIE 9148, 914897 (2014).